VERIFICATION OF THE CYCLOIDAL GEAR
TRAIN FAULT DIAGNOSIS METHODS BASED ON MEASURED DATA

Roman KRÓL[*][iD]**, Krzysztof OLEJARCZYK**[*][iD]**, Marcin WIKŁO**[*][iD]

*Faculty of Mechanical Engineering, Department of Applied Mechanics and Mechatronics,
Casimir Pulaski Radom University, ul. hm. kpt. Eugeniusza Stasieckiego 54, 26-600 Radom, Poland

r.krol@urad.edu.pl, k.olejarczyk@urad.edu.pl, m.wiklo@urad.edu.pl

Abstract: This article presents an experimental verification of various fault diagnosis methods for a cycloidal gear train. Measurements were performed on a laboratory test rig equipped with a cycloidal gearbox. Seven cycloidal discs with wear defects in successive lobes were manufactured using ABS material and mounted in a steel gearbox. For each cycloidal disc, the output torque was measured and analyzed with MATLAB algorithms to identify the number of defects. Previous research employed a multibody dynamics model of a cycloidal gear train, programmed in Fortran, to propose a new fault diagnosis method. However, experimental verification did not confirm the effectiveness of using only Morris Minimum Bandwidth Wavelets for diagnostic purposes. Therefore, several alternative methods were investigated: 1) adjustment of Morris wavelet parameters to match the general frequency characteristics of the analyzed gearbox, 2) Power Spectral Density (PSD) analysis, 3) methods based on PSD roll off and centroid, 4) analysis of narrowband-to-wideband energy ratios 5) spectral flatness analysis, 6) application of spectral entropy. Among the tested approaches, only spectral entropy enabled successful classification of the number of defects. Nevertheless, the entropy values were generally low, and the differences between certain defect cases were sensitive to noise interference. The successful application of spectral entropy for defect detection demonstrates that, in cycloidal gear trains – unlike in conventional cylindrical gears - defects in cycloidal discs lead to spectral scattering. This phenomenon represents a promising feature for future fault diagnosis methods.

Key words: cycloidal gear train, fault diagnosis, error diagnosis, teeth defects, spectral entropy, Morris Wavelets, Multibody Dynamics Method

1. INTRODUCTION

Contemporary research [1–13] on gearbox fault diagnosis focuses on multisensory measurements [1], spectral analysis [13,14], wavelet techniques [4,12], the development of compound methods and algorithms [12], feature fusion [3,14], filter applications [5], probabilistic approaches [3,6], adaptive stochastic resonance [7], angular position identification [8], spectral coherence [10], and other techniques aimed at ensuring the reliable operation of rotating machinery. Although gearbox diagnostics has a long history of methodological development, effective diagnostic approaches dedicated specifically to cycloidal gear trains remain limited [3,4,14–16].

In this article, the investigation of various spectral- and wavelet-based fault diagnosis methods led to the assumption that the defect geometry proposed in [4] induces spectral scattering. This phenomenon can be quantified using spectral entropy. A similar approach was presented in [15], where the authors concluded that defects in cycloidal discs influence the vibration spectrum. In particular, harmonic peaks accompanied by sidebands were observed and identified as potential diagnostic features.

In study [15], a rotation vector (RV) gearbox – comprising both a planetary stage and a cycloidal stage - was analyzed, and defects in the cycloidal disc were associated with distinct spectral peaks. In contrast, the present work focuses exclusively on a cycloidal gear reducer, without any additional stages. Attempts to extract diagnostic features using Morris Minimum Bandwidth Wavelets corresponding to specific harmonic frequencies – defined as the input shaft rotational frequency multiplied by the number of lobes or the number of pins in the pinwheel – were unsuccessful. Moreover, no clear pattern was observed in the vibration spectrum that could be directly associated with an increasing number of defects in the cycloidal disc.

Additionally, the analysis of the vibration signal envelope proved difficult to exploit, despite its successful application in distinguishing between a healthy cycloidal gearbox and one with a pin defect in [3].

Fault diagnosis attempts using Morris Minimum Bandwidth Wavelets [4], which have been widely applied in vibration signal analysis of rotating machinery also failed to reveal any consistent patterns that could support reliable defect identification.

The experimental data used for the investigation of fault diagnosis methods presented in this article were obtained from a laboratory test rig (Figure 1), consisting of: cycloidal gearbox with 16 external sleeves, 15 lobes, and 8 internal sleeves; two cycloidal discs; input and output shafts; a driving motor; a braking motor; and a torque measurement device. The measurement system was connected to National Instruments data acquisition cards interfaced with a notebook computer. An additional tachometer was used to measure the angular position of the cycloidal disc.

For each measurement, a cycloidal disc with a different number of defects was installed in the cycloidal gearbox. In total, eight

cycloidal discs were manufactured using a 3D printer from ABS material. One disc was defect-free, while the remaining seven discs contained from one to seven defects, respectively. Representative examples of disc without the defects and a defective one are shown in Figures 2 and 3.
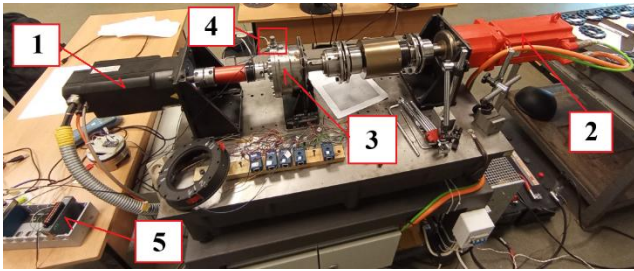

Fig. 1. Measurement rig. Driving motor (1), Braking motor (2), Cycloidal gearbox (3), Tachometer sensor (4), National Instruments data acquisition cards (5)

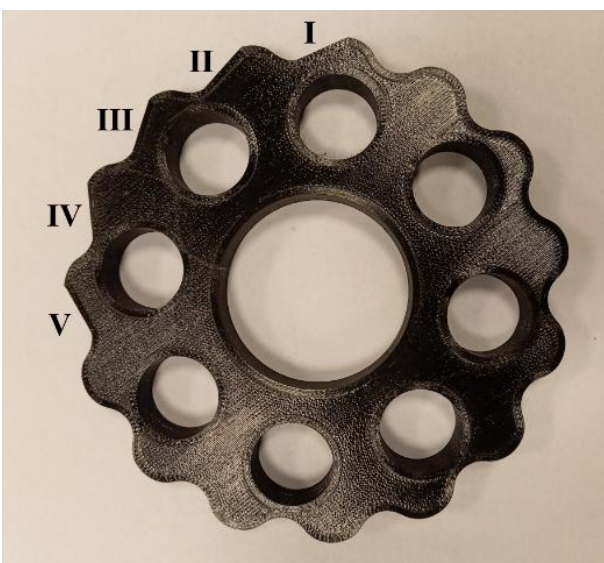**Fig. 2.** The defect-free ABS cycloidal disc

Fig. 3. The ABS cycloidal disc with 5 defects (I-V)

The defects introduced in the cycloidal discs were designed to simulate surface wear. Half of each lobe was replaced with a planar surface extending from the pit to the tip of the lobe. Contact with a surface of effectively infinite curvature radius leads to an increase in the contact force, which in turn affects the measured output torque.

The measured data were processed using MATLAB software, in which the fault diagnosis methods evaluated in this study were implemented. These methods included: 1) adjustment of Morris wavelet parameters to match the general frequency characteristics of the analyzed gearbox, 2) Power Spectral Density (PSD) analysis, 3) methods based on PSD roll off and spectral centroid, 4) analysis of narrowband-to-wideband energy ratios, 5) spectral flatness analysis, and 6) application of spectral entropy.

2. PARAMETERS OF THE MEASUREMENT SET UP

The structure of the cycloidal gearbox is shown in Figure 4. The parameters of the cycloidal discs are specified in Equation (1) and summarized in Table 1, while the parameters of the measurement rig are provided in Table 2.
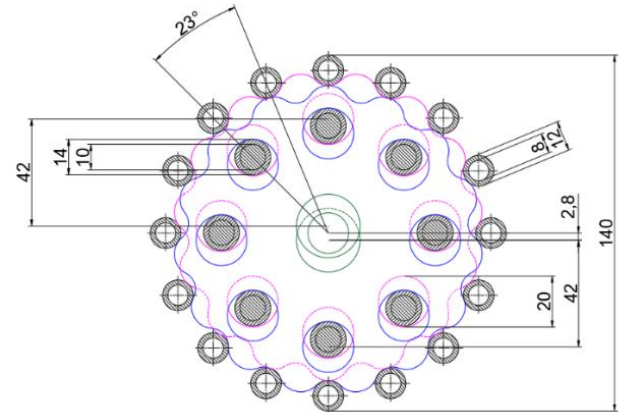

Fig. 4. Dimensions of the cycloidal gearbox used in the measurement set up

$$\begin{cases} x(t) = \dfrac{e \cdot z_k}{m}\cos(t) + e \cdot \cos(z_k \cdot t) - q \cdot \cos(t + \gamma) \\ y(t) = \dfrac{e \cdot z_k}{m}\sin(t) + e \cdot \sin(z_k \cdot t) - q \cdot \sin(t + \gamma) \\ \qquad \gamma = \operatorname{atan}\left[\dfrac{\sin(z_s \cdot t)}{\frac{1}{m} + \cos(z_s \cdot t)}\right] \end{cases}$$

(1)

Tab. 1. Parameters used in the equation (1)

Parameter	Description	Value
$x(t)$	Horizontal coordinate	-
$y(t)$	Vertical coordinate	-
t [rad]	Equation parameter	$0\text{-}2\pi$
e [m]	Eccentricity	0.0028
z_k	Number of external sleeves	16
z_s	Number of lobes	15
m	Short-width coefficient	0.7
q [m]	Radius of the external sleeve	0.006

Roman Król, Krzysztof Olejarczyk, Marcin Wikło
Verification of the Cycloidal Gear Train Fault Diagnosis Methods Based on Measured Data

DOI: 10.65731/ama/2026-0021

Tab. 2. Parameters of the measurement rig

Parameter	Description	Value
M	Moment of the braking motor	22 Nm
f	Sampling frequency	25.6 kHz
ω	Angular velocity of the input shaft	500 RPM

During the measurements, the braking motor torque was not constant. Although it was set to a nominal value of 22 Nm, significant fluctuations were observed. These fluctuations were filtered using a high-pass filter implemented in MATLAB. Cut-off frequencies of 0.5 Hz, 1 Hz, 10 Hz and 50 Hz were applied. Unfortunately, the elimination of low frequency components led to significant difficulties in verifying the proposed methods. Low-frequency components are more important in the measured data than in the data obtained from the Fortran simulation model. Moreover, the high-frequency peaks in the FFT spectrum of the measured data were significantly lower than those obtained in the simulations. Therefore, all methods were ultimately tested on the unfiltered measured data, which include low-frequency fluctuations of the braking motor torque.

3. MULTIBODY DYNAMICS MODEL PROGRAMMED IN FORTRAN

GNU Fortran was used to implement multibody dynamics model of the cycloidal gearbox with parameters given in Figure 4, Equation 1 and Table 1. The model was employed to verify the measured signals. In the simulations, the system of equations (2) is integrated using 2nd order Runge Kutta method.

$$\begin{bmatrix} M & -D^T \\ D & 0 \end{bmatrix} \begin{bmatrix} \ddot{u} \\ \lambda \end{bmatrix} = \begin{bmatrix} F \\ \gamma \end{bmatrix}, \tag{2}$$

where: M – is the mass matrix (contains masses and moments of inertia of the system components), D – is the Jacobian matrix, 0 – denotes the zero matrix, $\ddot{u}$ – represents the solved accelerations, λ – denotes the solved reaction forces, F – is the vector of applied forces and moments, γ – is the right-hand side vector of the acceleration equations.

The bodies in the multibody dynamics model are allowed to rotate about their mounting points, which are modeled as revolute joints. Friction in the joints was neglected. Contact interactions were modeled using the Hunt-Crossley Hertzian contact model (3), with parameters listed in Table 3.

$$F_n = K \cdot \delta^p \pm C \cdot v_n, \tag{3}$$

where: F_n – is the normal contact force, K – is the contact stiffness, δ – is the penetration depth, p – is the force exponent, C – is the viscous damping coefficient, and v_n - is the normal velocity, defined as the relative velocity of the contacting points.

The cycloidal discs in the multibody dynamics model were discretized using uniform increments of the parameter t in the cycloidal disc equation (1).

Tab. 3. Hertzian contact parameters in the Fortran model

Parameter	Description	Value
K	Contact stiffness [N/m$^{1.5}$]	Curvature and material dependent
E	Young modulus [MPa]	2200 (analysis with ABS disc)
		200 000 (analysis with steel disc)
υ	Poisson's ratio	0.37 (analysis with ABS disc)
		0.3 (analysis with steel disc)
C	Contact viscous damping [Ns/m]	20 (analysis with ABS disc)
		200 (analysis with steel disc)
p	Force exponent	1.5

4. MEASURED DATA

Measurements were conducted using a single cycloidal gearbox, tested in both a healthy configuration and with cycloidal discs containing defects. The gearbox was operated with seven consecutive discs exhibiting an increasing number of defects. In the first disc, a defect was present in a single lobe; in the second disc, defects were present in two consecutive lobes; in the third disc, three consecutive lobes were defective, and so on. The parameters of the measured signals are summarized in Table 4.

Tab. 4. Parameters of the measured data

Parameter [Nm]	No defect	1 defect	2 defects	3 defects
Min	12.88	10.89	10.56	9.839
Max	42.76	42.87	39.86	42.77
Mean	22.03	22.86	22.71	22.37
Std dev.	2.912	4.964	4.557	4.047
Range	29.88	31.99	29.3	32.93

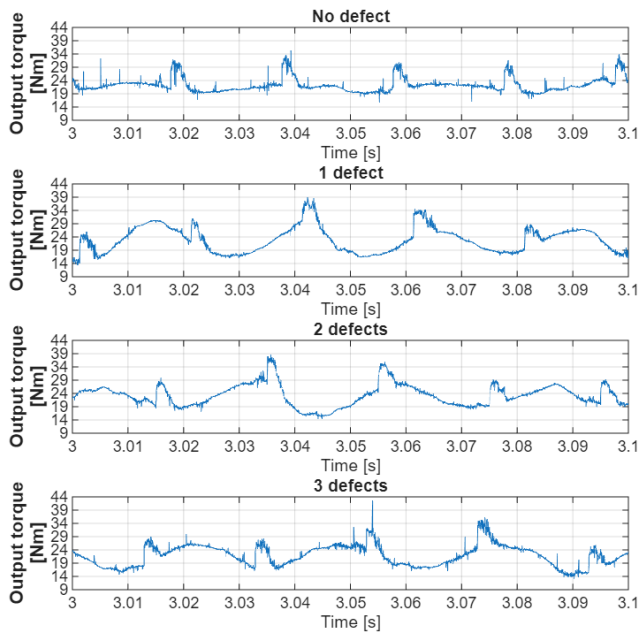| Parameter [Nm]	4 defects	5 defects	6 defects	7 defects
Min	11.05	10.7	13.52	10.86
Max	38.8	38.25	38.5	42.14
Mean	22.8	22.28	22.83	22.17
Std dev.	4.232	4.125	3.923	3.462
Range	27.75	27.55	24.97	31.28

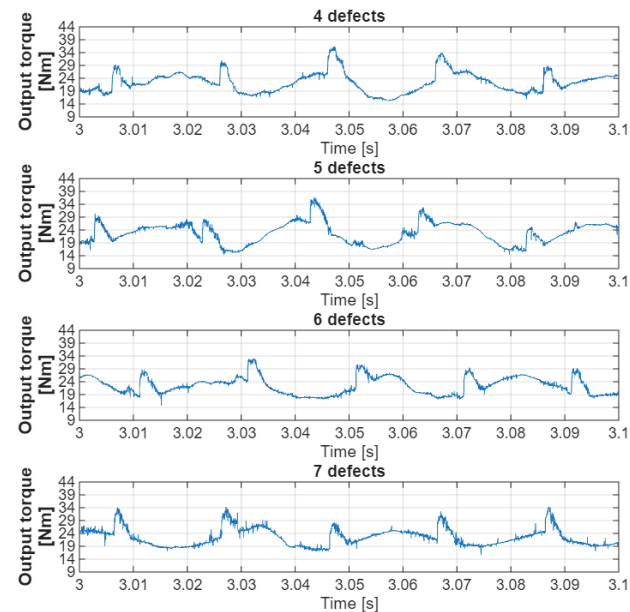**Fig. 5.** Measured signals for no defect and for 1-3 defects

Fig. 6. Measured signals for 4-7 defects

The measured signals are presented in Figures 5 and 6. The corresponding time-domain plots exhibit a drifting DC component of the output torque, which is caused by fluctuation in the braking motor. Figures 7 and 8 present the output torque obtained for the same gearbox configuration using the Fortran-based multibody dynamics model with ABS disc (Figure 7) and with steel disc (Figure 8). The simulated output torque signals are more symmetric and exhibit lower peak-to-peak amplitudes, however the influence of the defects is difficult to distinguish in the general observation.

In the Fortran model, the time increment was constant and equal to $\Delta t=10^{-5}$ s, corresponding to a sampling rate of 100 kHz. However, in the presented data every 10-th iteration is shown. The output torque measured using National Instruments data acquisition cards was sampled at 25.6 kHz, as specified in Table 2. The higher temporal resolution of the Fortran simulation enables more accurate capture of output torque modulation resulting from rolling contact interactions. Nevertheless, testing Morris wavelets on the

Fortran model, as reported in [4], did not lead to a clear formulation of a reliable fault diagnosis method.
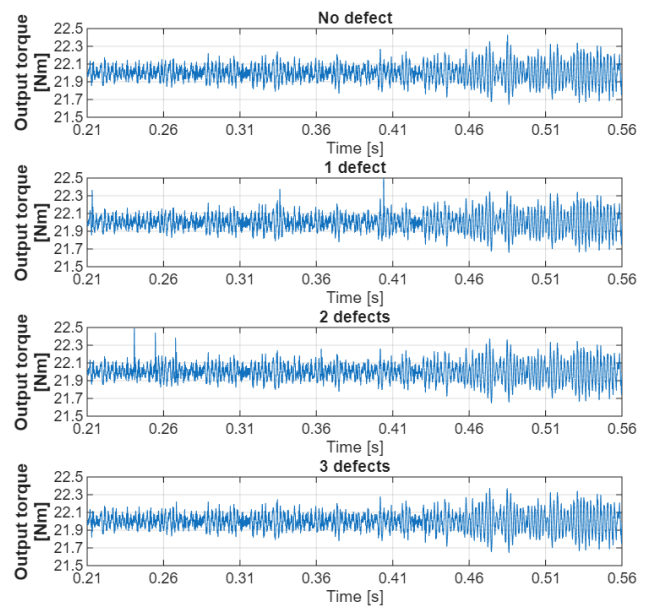

Fig. 7. Data solved in the Fortran model (0-3 defects) in the analysis with ABS disc
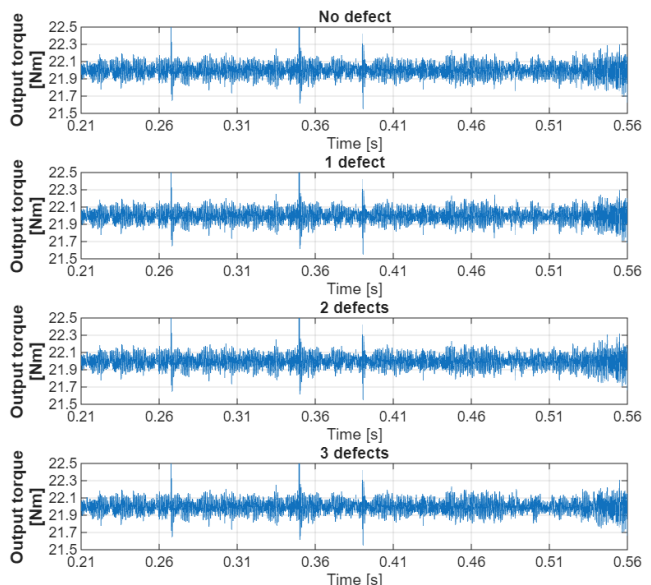

Fig. 8. Data solved in the Fortran model (0-3 defects) in the analysis with steel disc

Based on the measured data, new fault diagnosis approaches were investigated.

5. TESTING NEW FAULT DIAGNOSIS METHODS

Morris Minimum Bandwidth Wavelets are commonly used in the diagnosis of planetary gearboxes. In previous studies [4], certain features enabled discrimination between selected numbers of defects. In the present work, further analysis was conducted with attempts to adjust the frequency characteristics of the measured output torque to the computed scalograms. Unfortunately, this approach proved unsuccessful for the analyzed cycloidal gearbox

Roman Król, Krzysztof Olejarczyk, Marcin Wikło
Verification of the Cycloidal Gear Train Fault Diagnosis Methods Based on Measured Data

DOI: 10.65731/ama/2026-0021

geometry.

5.1. Adjustment of the Morris wavelets parameters

For the vibration signals measured for the healthy gearbox and for the gearbox equipped with defective cycloidal discs, the rotational frequency of the input shaft was determined as 8.33 Hz (500 RPM). Based on this value, the gear meshing frequency was calculated as 8.33 Hz multiplied by the number of pins. Next, using the maximum allowable Morris wavelet decomposition level, the frequency bandwidths of each detail level were determined as $B_{LO}=fs/2^{j+1}$ and $B_{HI}=fs/2^j$, where j denotes the wavelet decomposition level. The decomposition level j for which the meshing frequency fell within the corresponding bandwidth was selected. This level was assumed to contain components associated with potential defects. Subsequently, the signal envelope at the selected level was extracted using Hilbert transform, and the FFT of the envelope was computed. Finally, the envelope spectra of the healthy gearbox and the defective gearbox were compared in order to identify fault-related harmonic components. However, this method was unable to distinguish between different numbers of defects in the measured signals.

An additional approach using Morris wavelets was also investigated. For the healthy gearbox and for the seven cycloidal discs with defects, Morris Minimum-Bandwidth Wavelets scalograms were computed in MATLAB. According to [4], the minimum values of scalograms were compared with the minimum values obtained for the measurement corresponding to the highest number of defects (seven defects). The objective of this approach was to identify minima overlapping with the largest gap in the defect sequence.

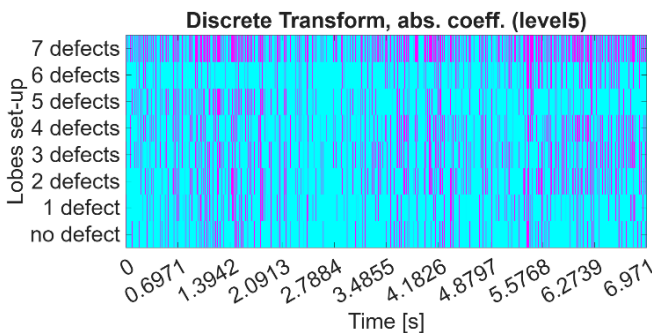The comparison of the minima for all scalograms is shown in Figure 9.

Fig. 9. Minima of scalograms (dark colour), which overlap with the minima of scalogram for the 7 defects

The scalograms shown in Figure 9 indicate that Morris Minimum-Bandwidth Wavelets do not exhibit a gradual relationship between the number of defects and the number of overlapping minima. Attempts to identify such a relationship at other decomposition levels also did not yield positive results.

5.2. Application of the coherence function

The magnitude square coherence for the amplitude of the output torque [Nm] was calculated using MATLAB *mscohere* function. No gradual dependence was observed in the coherence functions presented in Figures 10 and 11. The coherence function yields values in the range from 0 to 1, which reflect the similarity between the harmonic components of the healthy gearbox signal and those of the defective gearbox signal.
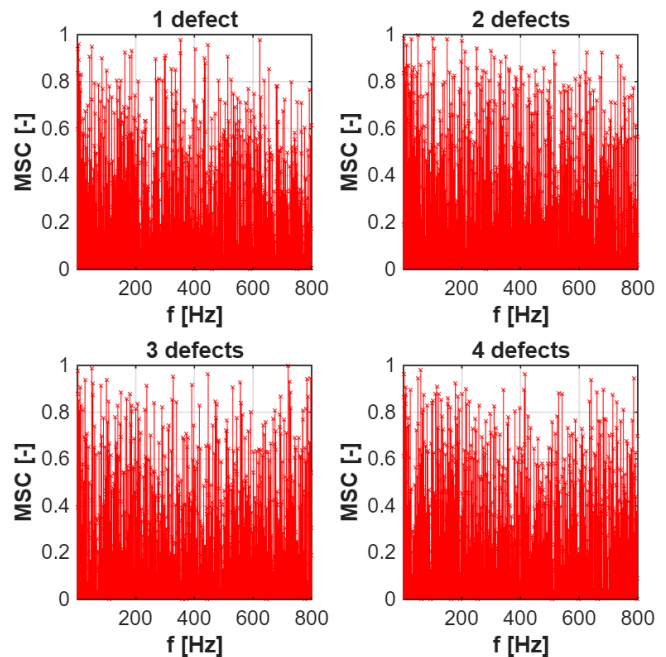

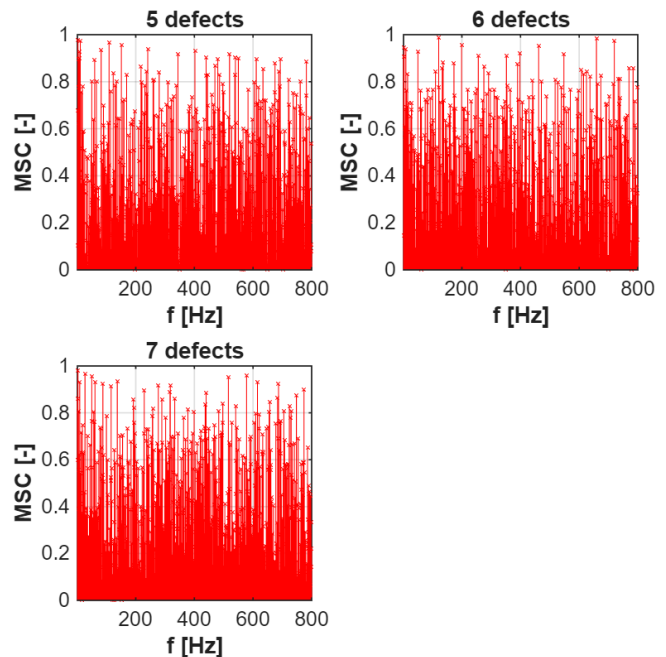**Fig. 10.** Coherence function for the healthy gearbox and gearbox with 1-4 defects

Fig. 11. Coherence function for the healthy gearbox and gearbox with 5-7 defects

5.3. Analysis of Power Spectral Density (PSD)

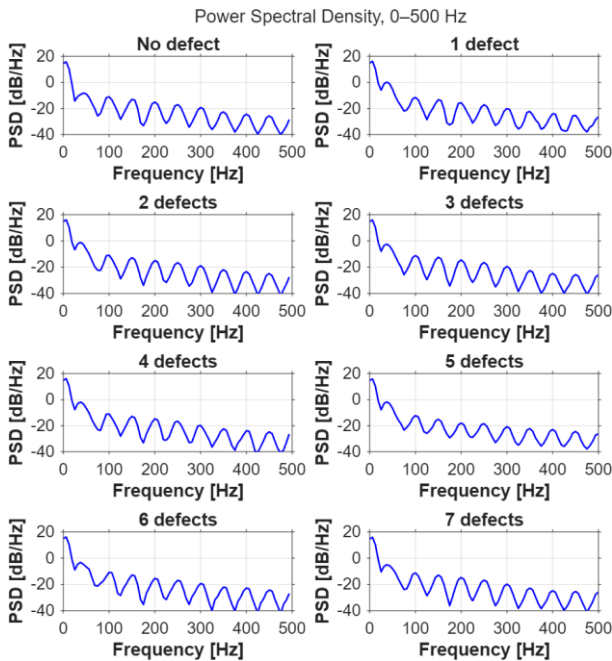In the MATLAB environment, the PSD was computed for each measured signal using the *pwelch* function.

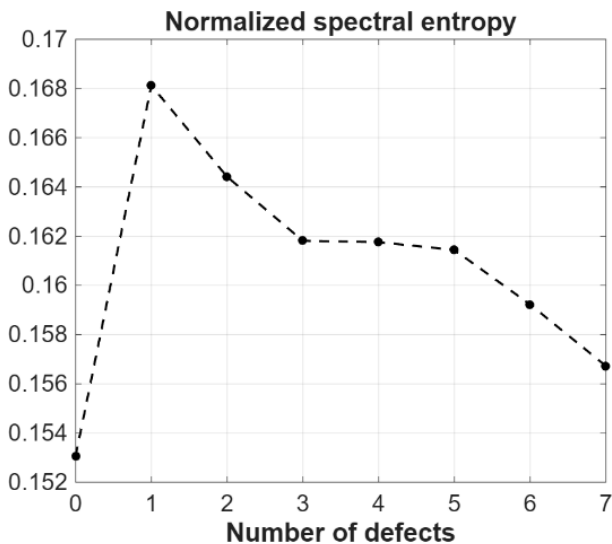**Fig. 12.** Power spectral density of the measured output torques

Fig. 13. Normalized spectral entropy for 0-7 defects

The PSD plots do not exhibit gradual features that could be used to determine the number of defects. However, the spectral entropy computed using Equations (4)-(7) proved to be effective in identifying the number of defects present in the measured signal.

$$P_{norm} = \frac{P_{xx}}{\sum P_{xx}} \tag{4}$$

$$H = -\sum P_{norm} \cdot log_2(P_{norm} + \epsilon) \tag{5}$$

$$H_{max} = log_2 N, \tag{6}$$

$$E = \frac{H}{H_{max}}. \tag{7}$$

where: P_{xx} – denotes the PSD (Figure 12), P_{norm} – is the normalized PSD, ϵ- is a small constant introduced to avoid taking the logarithm of zero, H – represents the spectral entropy, H_{max} – is the maximum possible entropy, and E – is normalized entropy.

The calculated entropy values enable correct identification of the number of defects; however, for cases with three and four

defects, the differences between the normalized entropy values are negligible.

5.4. Methods using roll-off and centroid of PSD

It was assumed that increase in medium frequency of each time window indicate appearance of the high frequencies, which indicate emergence of defects. The rise in centroid will indicate, that signal energy shifts towards the high frequencies. The second indicator, Roll-off 95% is the boundary frequency. Below this value 95% of the signal energy is concentrated. The red, dashed line in Figure 14 is the Roll-off 95% value versus time. The rise in roll-off 95% allow for detection of the high frequencies that emerge in the signal. This can be caused by the appearance of high frequencies due to defects.
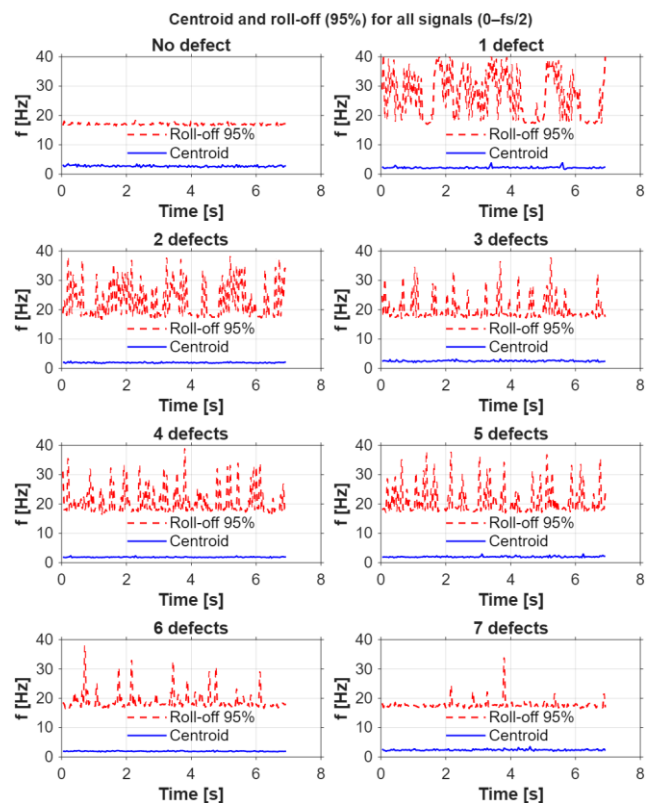

Fig. 14. Roll-offs 95% and centroids for the measured signals

Representative centroid values for the healthy gearbox and for configurations with 1-7 defects are listed in Table 5.

Tab. 5. Exemplary centroid values from Figure 14.

Number of defects	Centroid value
0	2.82
1	2.241
2	1.88
3	2.95
4	1.8
5	2.06
6	1.88
7	2.27

Roman Król, Krzysztof Olejarczyk, Marcin Wikło
Verification of the Cycloidal Gear Train Fault Diagnosis Methods Based on Measured Data

DOI: 10.65731/ama/2026-0021

There is no clear or gradual dependence between the spectral centroid and the number of defects in the gearbox. Similarly, the roll-off frequency does not exhibit features that would allow determination of the number of defects based on the occupied frequency range.

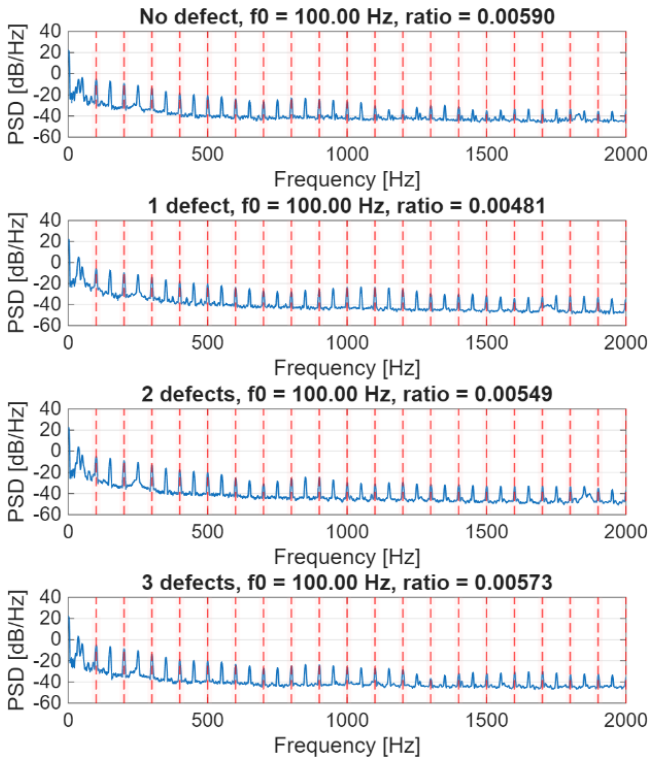## 5.5. Searching for the narrowband-to-wideband energy ratios

Fig. 15. Power Spectral Density divided in narrowband (for the healthy gearbox and defects 1-3)
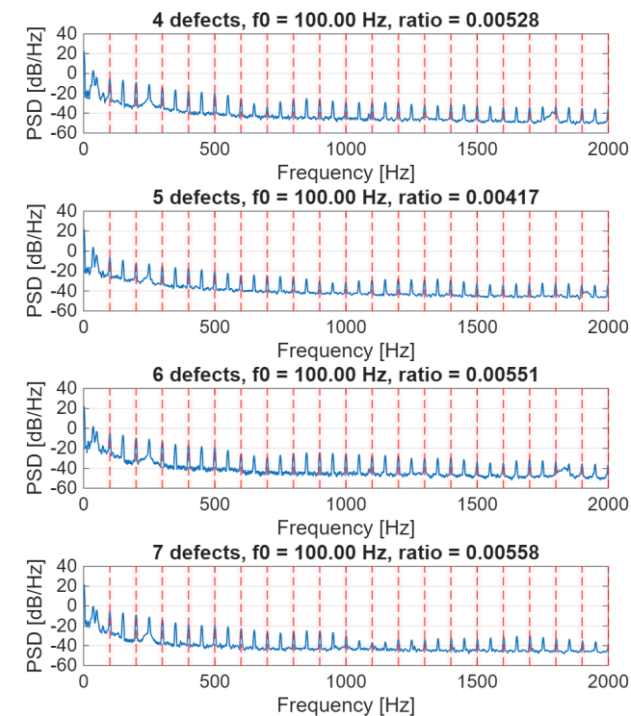

Fig. 16. Power Spectral Density divided in narrowband (for defects 4-7)

An important feature of the PSD in fault diagnosis is localization of spectral energy within harmonic components or narrow frequency bands. For periodic signals, energy is primarily concentrated in harmonic components; however, in gearboxes, defects may cause an increase in spectral energy within narrowbands, leading to a broader PSD. Therefore, it is useful to examine the ratio of narrowband energy to the total signal energy. The base frequency for the harmonics was set to $f_0=100$ Hz, and the harmonic energy was computed for frequencies equal to $n \cdot f_0$, where n is an integer. The calculated energy ratios are presented for each case in Figure 16, and their values are additionally summarized in the bar chart shown in Figure 17.

There is also no gradual dependence between the number of defects and the data presented in Figure 16. Consequently, it is not possible to determine the number of defects based on the energy ratio.
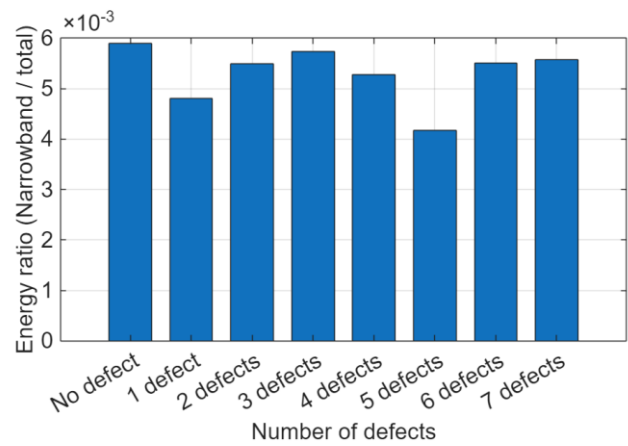

Fig. 17. Narrowband/Total spectral energy ratio for the PSD presented in Figures 15 and 16

5.6. Analysis of spectral flatness and application of spectral entropy

Figure 13 presents the normalized entropy results. In this section, Shannon entropy (expressed in bits) and spectral flatness were investigated. Shannon entropy proved capable of classifying the number of defects present in the measured signal. However, in its normalized form, the entropy values for signals with three and four defects were nearly identical. As a result, the differences between these cases are small, and the method may fail under conditions of high noise levels in the measured signals.

Spectral flatness was computed as the ratio of geometric mean to the arithmetic mean of the PSD. Unfortunately, spectral flatness was not able to determine the number of defects in the measured signals.

The Shannon spectral entropy presented in Figure 18 was computed without normalization, according to Equation (8). Spectral flatness was calculated using Equation (9).

$$H = -\sum P_{norm}(f_i) log_2 P_{norm}(f_i), \tag{8}$$

$$F = \frac{[\prod P(f_i)]^{\frac{1}{N}}}{\frac{1}{N}[\sum P(f_i)]}, \tag{9}$$

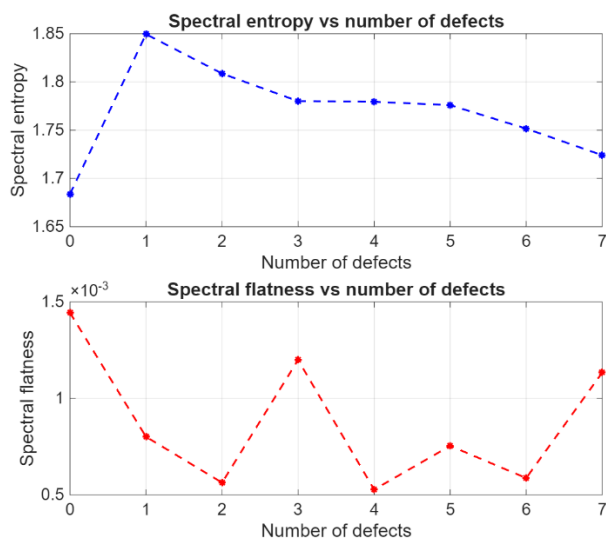The calculated spectral entropy values are listed in Table 6.

Fig. 18. Spectral entropy and spectral flatness for measured signals

Tab. 6. Spectral entropy values for the measured signals

Number of defects	Spectral Entropy
0	1.6838
1	1.8495
2	1.8087
3	1.7801
4	1.7794
5	1.776
6	1.7516
7	1.7241

Among the investigated methods, Shannon spectral entropy proved to be only reliable approach for determining the number of defects in the measured signals (output torque).

6. COMPARISON OF SIMULATIONS WITH ABS AND STEEL DISCS

The simulation data were examined for the strictly monotonically decreasing Shannon spectral entropy. The frequency bands for which this condition was satisfied are presented in Figure 19. The lower limits of the bands are connected by a blue dashed line, while the upper limits are marked with a red dashed line.

In contrast, no strictly monotonically decreasing entropy was observed in the data obtained from the simulation with the ABS disc. A possible hypothesis explaining this phenomenon is related to the Hunt and Crossley contact model, which incorporates both spring and a damper. In the FFT spectrum shown in Figure 20, increased amplitudes can be observed in the range of 400-500 Hz for the simulation with the ABS disc, which are not present in the spectrum obtained from the simulation with the steel disc. These increased peaks are also not observed in the FFT of the measured data, in which the high-frequency components exhibit significantly lower amplitudes than those obtained in both simulations.
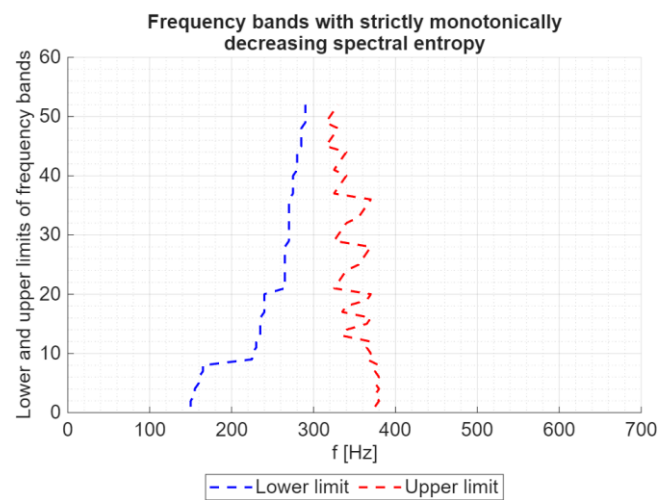

Fig. 19. Frequency band limits, for which the Shannon spectral entropy is strictly monotonically decreasing (Fortran simulation for steel discs)
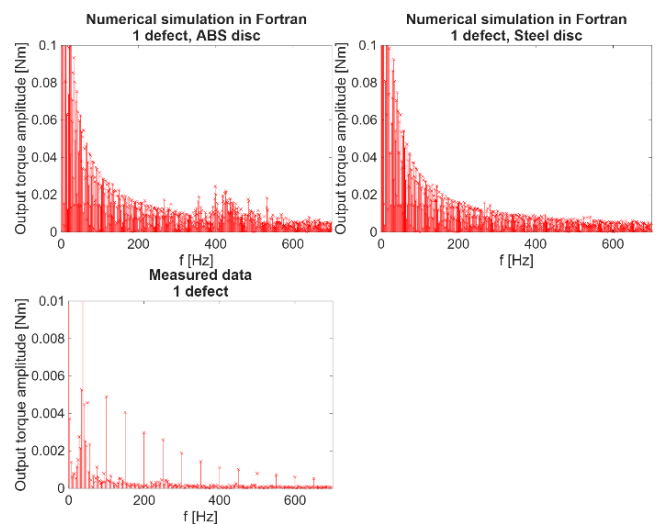

Fig. 20. FFT spectra for the Fortran simulations with ABS and steel discs and for the measured data with one defect

7. DISCUSSION OF RESULTS

Cycloidal gearboxes are mechanisms whose dynamic characteristics differ significantly from those of conventional gearboxes. Their dynamic behavior is strongly influenced by backlash [13] and contact parameters. The output torque is modulated by rolling contact phenomena, which increases the complexity of the spectral characteristics of both the input and output torque signals. The defects introduced in this study, initially designed in numerical research, lead to increased contact forces. Consequently, disturbances in the output torque are expected to exhibit harmonic behavior. The defects were distributed across successive lobes, and it was initially assumed that such defects could be easy identified through feature extraction from the signal spectrum. However, spectral analysis did not reveal any promising relationship between spectral features and the number of defects. The application of Morris Minimum Bandwidth Wavelets, which are widely used in fault diagnostics of rotating machinery, also failed to provide useful features when analyzing the scalograms. Further analysis of the PSD indicated that spectral entropy is the most reliable classification method for this type of defect. Nevertheless, an initial inspection of

Roman Król, Krzysztof Olejarczyk, Marcin Wikło
Verification of the Cycloidal Gear Train Fault Diagnosis Methods Based on Measured Data

DOI: 10.65731/ama/2026-0021

the PSD plots did not reveal any clear features that could distinguish between different numbers of defects.

The hypothesis of spectral scattering was first investigated using PSD analysis. The ratio of narrowband energy to the total signal energy was examined under the assumption that the signal from a healthy gearbox should exhibit predominantly harmonic characteristics, whereas the emergence of defects would cause energy scattering around successive harmonics. However, the rolling contact in cycloidal gearboxes does not lead to the appearance of single, clearly distinguishable spectral peaks. Instead, the spectral characteristics of cycloidal gearboxes are highly complex. Analysis of the narrowband-to-total energy ratio did not reveal any useful diagnostic features, as the energy ratios appeared random with increasing numbers of defects.

Analysis of the spectral centroid and the 95% roll-off frequency did not lead to successful development of a method capable of distinguishing between different numbers of defects. In cycloidal gearboxes, the introduction of defects in the cycloidal discs alters the spectrum; however, no clear relationship was observed between the increasing number of defects and the amount of high-frequency content in the signal. Consequently, the spectral centroid values for signals with successive defects appear random. Similarly, the 95% roll-off frequency does not provide reliable features for classifying the number of defects.

The introduction of the defects into the cycloidal disc lead to emergence of short impulse disturbances, which cause changes in the measured output torque signal and result in a broader spectrum. The PSD becomes more evenly distributed. Spectral entropy is capable of capturing these disturbances by quantifying the degree of spectral disorder in the measured signal. A comparison of the analyzed diagnostic methods is presented in Table 7.

8. CONCLUSIONS

Cycloidal gearboxes exhibit complex spectral characteristics in the output torque signal. Defects in the cycloidal disc introduce disturbances with a broadband spectral content. Among the investigated approaches, Shannon spectral entropy proved to be the most effective method for defect classification. The measured signals confirm the validity of this approach. However, in the presence of high noise levels, the calculated spectral entropy values may be suppressed, which can reduce classification reliability.

Tab. 7. Comparison of the investigated fault diagnosis methods for the cycloidal gearbox

Method	Remarks
Morris Minimum-Bandwidth wavelets	Feature extraction is very difficult and does not provide reliable diagnostic indicators
Coherence function	No consistent trend is observed in the coherence functions calculated for successive defect cases
PSD	PSD plots do not reveal features useful for defect classification; however, they serve as a basis for spectral entropy calculation
Centroid and 95% roll-off	Neither the spectral centroid nor the 95% roll-off frequency enables reliable classification of the number of defects. This method would be effective if defects
	introduced distinct high-frequency components
Narrowband-to-total energy ratio	No clear dependence is observed between the narrowband energy and the number of defects
Spectral flatness	Spectral flatness is easy to compute but unsuccessful to defect classification
Normalized spectral entropy	This method is partially effective; however, normalization reduces its sensitivity to defect severity
Shannon spectral entropy	This method provides reliable classification; however, high noise levels may lead to misclassification

REFERENCES

1. Fu Y, Chen X, Liu Y, Son C, Yang Y. Gearbox Fault Diagnosis Based on Multi-Sensor and Multi-Channel Decision-Level Fusion Based on SDP. Applied Sciences (Switzerland). 2022;12(15). https://doi.org/10.3390/app12157535
2. Xie F, Liu H, Dong J, Wang G, Wang L, Li G. Research on the Gearbox Fault Diagnosis Method Based on Multi-Model Feature Fusion. Machines. 2022;10(12). https://doi.org/10.3390/machines10121186
3. Komorska I, Olejarczyk K, Puchalski A, Wikło M, Wołczyński Z. Fault Diagnosing of Cycloidal Gear Reducer Using Statistical Features of Vibration Signal and Multifractal Spectra. Sensors. 2023;23(3). https://doi.org/10.3390/s23031645
4. Król R. Analysis of the single stage cycloidal gearbox with lobe defects. Fault diagnosis attempts using coherence function and Morris minimum-bandwidth wavelets. Archive of Mechanical Engineering. 2023;70(3):409-431. https://doi.org/10.24425/ame.2023.146846
5. Li Y, Feng K, Liang X, Zuo MJ. A fault diagnosis method for planetary gearboxes under non-stationary working conditions using improved Vold-Kalman filter and multi-scale sample entropy. J Sound Vib. 2019;439:271-286. https://doi.org/10.1016/j.jsv.2018.09.054
6. Schmidt S, Heyns PS, de Villiers JP. A novelty detection diagnostic methodology for gearboxes operating under fluctuating operating conditions using probabilistic techniques. Mech Syst Signal Process. 2018;100:152-166. https://doi.org/10.1016/j.ymssp.2017.07.032
7. Lei Y, Han D, Lin J, He Z. Planetary gearbox fault diagnosis using an adaptive stochastic resonance method. Mech Syst Signal Process. 2013;38(1):113-124. https://doi.org/10.1016/j.ymssp.2012.06.021
8. D'Elia G, Mucchi E, Cocconcelli M. On the identification of the angular position of gears for the diagnostics of planetary gearboxes. Mech Syst Signal Process. 2017;83:305-320. https://doi.org/10.1016/j.ymssp.2016.06.016
9. Chen X, Feng Z. Time-frequency space vector modulus analysis of motor current for planetary gearbox fault diagnosis under variable speed conditions. Mech Syst Signal Process. 2019;121:636-654. https://doi.org/10.1016/j.ymssp.2018.11.049
10. Schmidt S, Heyns PS, Gryllias KC. A methodology using the spectral coherence and healthy historical data to perform gearbox fault diagnosis under varying operating conditions. Applied Acoustics. 2020;158:107038. https://doi.org/10.1016/j.apacoust.2019.107038
11. Zhang D, Yu D. Multi-fault diagnosis of gearbox based on resonance-based signal sparse decomposition and comb filter. Measurement (Lond). 2017;103:361-369. https://doi.org/10.1016/j.measurement.2017.03.006
12. Teng W, Ding X, Cheng H, Han C, Liu Y, Mu H. Compound faults diagnosis and analysis for a wind turbine gearbox via a novel vibration model and empirical wavelet transform. Renew Energy. 2019;136:393-402. https://doi.org/10.1016/j.renene.2018.12.094
13. Król R. Analysis of the backlash in the single stage cycloidal gearbox. Archive of Mechanical Engineering. 2022;69(4):693-711. https://doi.org/10.24425/ame.2022.141521
14. Qiao Y, Wang H, Cao J, Lei Y. Sound-vibration spectrogram fusion

method for diagnosis of RV reducers in industrial robots. Mech Syst Signal Process. 2024;214:111411.
https://doi.org/10.1016/j.ymssp.2024.111411

15. E Y, Liu Z, Chen H, et al. Dynamic modeling and vibration analysis for fault diagnosis of rotate vector reducers. Mech Syst Signal Process. 2025;224:111965. https://doi.org/10.1016/j.ymssp.2024.111965

16. Guo D, Zhang Y, Chen X, et al. Data-driven fault identification method of RV reducer used in industrial robot. Heliyon. 2024;10(22). https://doi.org/10.1016/j.heliyon.2024.e40115

Roman Król: https://orcid.org/0000-0002-6279-9562

Krzysztof Olejarczyk: https://orcid.org//0000-0002-9055-161X

Marcin Wikło: https://orcid.org//0000-0001-5210-6657